

1 Evasion of Neutralizing Antibody Response by the SARS-CoV-2 BA.2.75 Variant

2

3 Panke Qu<sup>1,2,#</sup>, John P. Evans<sup>1,2,3,#</sup>, Yi-Min Zheng<sup>1,2</sup>, Claire Carlin<sup>4</sup>, Linda J. Saif<sup>5,6,7</sup>,

4 Eugene M. Oltz<sup>8</sup>, Kai Xu<sup>1,2</sup>, Richard J. Gumina<sup>4,9,10</sup>, and Shan-Lu Liu<sup>1,2,7,8\*</sup>

5

6 <sup>1</sup>Center for Retrovirus Research, The Ohio State University, Columbus, OH 43210, USA

7 <sup>2</sup>Department of Veterinary Biosciences, The Ohio State University, Columbus, OH 43210, USA

8 <sup>3</sup>Molecular, Cellular, and Developmental Biology Program, The Ohio State University,  
9 Columbus, OH 43210, USA

10 <sup>4</sup>Department of Internal Medicine, Division of Cardiovascular Medicine, The Ohio State  
11 University, Columbus, OH 43210, USA

12 <sup>5</sup>Center for Food Animal Health, Animal Sciences Department, OARDC, College of Food,  
13 Agricultural and Environmental Sciences, The Ohio  
14 State University, Wooster, OH 44691, USA

15 <sup>6</sup>Veterinary Preventive Medicine Department, College of Veterinary Medicine, The Ohio State  
16 University, Wooster, OH 44691, USA

17 <sup>7</sup>Viruses and Emerging Pathogens Program, Infectious Diseases Institute, The Ohio State  
18 University, Columbus, OH 43210, USA

19 <sup>8</sup>Department of Microbial Infection and Immunity, The Ohio State University, Columbus, OH  
20 43210, USA

21 <sup>9</sup>Dorothy M. Davis Heart and Lung Research Institute, The Ohio State University Wexner  
22 Medical Center, Columbus, OH 43210, USA

23 <sup>10</sup>Department of Physiology and Cell Biology, College of Medicine, The Ohio State University  
24 Wexner Medical Center, Columbus, OH  
25 43210, USA

26

27

28 #Authors contributed equally to this work

29 \*Corresponding Author: [liu.6244@osu.edu](mailto:liu.6244@osu.edu)

30

31 **Abstract**

32           The newly emerged BA.2.75 SARS-CoV-2 variant exhibits an alarming 9 additional  
33 mutations in its spike (S) protein compared to the ancestral BA.2 variant. Here we examine the  
34 neutralizing antibody escape of BA.2.75 in mRNA-vaccinated and BA.1-infected individuals, as  
35 well as the molecular basis underlying functional changes in the S protein. Notably, BA.2.75  
36 exhibits enhanced neutralization resistance over BA.2, but less than the BA.4/5 variant. The  
37 G446S and N460K mutations of BA.2.75 are primarily responsible for its enhanced resistance to  
38 neutralizing antibodies. The R493Q mutation, a reversion to the prototype sequence, reduces  
39 BA.2.75 neutralization resistance. The mutational impact is consistent with their locations in  
40 common neutralizing antibody epitopes. Further, the BA.2.75 variant shows enhanced cell-cell  
41 fusion over BA.2, driven largely by the N460K mutation, which enhances S processing. Structural  
42 modeling revealed a new receptor contact introduced by N460K, supporting a mechanism of  
43 potentiated receptor utilization and syncytia formation.

44

## 45 Introduction

46 Emergence of the Omicron variant of SARS coronavirus 2 (SARS-CoV-2) in late 2021  
47 sparked an unprecedented wave of coronavirus disease 2019 (COVID-19) cases and exhibited  
48 robust evasion of vaccine- and infection-induced immunity (Gruell et al., 2022; Hoffmann et al.,  
49 2022). More recently, several subvariants of Omicron have been identified, which have driven  
50 subsequent waves of infection. The BA.1 subvariant, responsible for the initial Omicron wave,  
51 was replaced by BA.2, which displayed slightly enhanced transmissibility and resistance to BA.1-  
52 induced sera (Centers for Disease Control and Prevention, 2022; Evans et al., 2022; Yamasoba  
53 et al., 2022b). BA.2 then evolved into several progeny subvariants, including the BA.2.12.1 variant,  
54 which subsequently became predominant (Centers for Disease Control and Prevention, 2022).  
55 Remarkably, the BA.4 and BA.5 variants, which bear identical spike (S) proteins and evolved from  
56 BA.2, are currently dominant in the world, including in the US (Centers for Disease Control and  
57 Prevention, 2022). BA.4 and BA.5 bear an L452R mutation that is primarily responsible for further  
58 enhanced neutralizing antibody resistance (Qu et al., 2022; Tuekprakhon et al., 2022). Recently,  
59 another distinct BA.2-derived subvariant, BA.2.75, has been identified. BA.2.75 is increasing in  
60 prevalence in southeast Asia and has been detected globally (Callaway, 2022). Notably, BA.2.75  
61 bears 9 key S mutations including K147E, W152R, F157L, I210V, G257S, D339H, G446S, and  
62 N460K, as well as an R493Q reversion mutation (World Health Organization, 2022) (**Fig. 1A**).  
63 These mutations, particularly those in the receptor binding domain (RBD), have generated  
64 concern over further immune escape.

65 Here we characterize the BA.2.75 S protein by examining its sensitivity to neutralizing  
66 antibodies from mRNA-vaccinated and/or boosted health care workers (HCWs), as well as from  
67 Omicron-wave-hospitalized COVID-19 patients. In addition, we examine BA.2.75 infectivity, S  
68 processing, and fusogenicity. Mutational analysis revealed the N460K as a key driver of enhanced  
69 fusogenicity, while the G446S and N460K mutations were primarily responsible for reduced  
70 neutralization sensitivity of BA.2.75 compared to BA.2. Moreover, we find that the R493Q

71 reversion mutation enhances the neutralization sensitivity of BA.2.75. These findings inform our  
72 understanding of SARS-CoV-2 evolution and will aid in addressing the ongoing threat of emerging  
73 SARS-CoV-2 variants.

74

## 75 **Results**

76 *BA.2.75 exhibits enhanced neutralization resistance over BA.2.*

77 We first sought to characterize sensitivity to vaccine-induced immunity of the BA.2.75  
78 variant. Utilizing our previously reported pseudotyped lentivirus assay (Zeng et al., 2020), we  
79 examined neutralizing antibody (nAb) titers for 15 Ohio State University Wexner Medical Center  
80 health care workers (HCWs) in serum samples collected 3-4 weeks after vaccination with a  
81 second dose of Moderna mRNA-1273 (n = 7) or Pfizer/BioNTech BNT162b2 (n = 8) vaccine, and  
82 1-12 weeks after vaccination with a homologous booster dose (see STAR Methods). Patient sera  
83 were examined for nAb titers against lentivirus pseudotyped with S from ancestral SARS-CoV-2  
84 S bearing only the D614G mutation, as well as S from BA.1, BA.2, BA.2.12.1, BA.4/5, and BA.2.75  
85 (Fig. 1A). All S constructs were functional and produced comparably infectious lentivirus  
86 pseudotypes (Fig. 1B).

87 Notably, all Omicron sublineages, including BA.2.75, exhibited strong resistance to 2-  
88 dose-induced immunity compared to D614G ( $p < 0.0001$ ), with only 1-2 HCW samples exhibiting  
89 50% neutralization titers ( $NT_{50}$ ) above the limit of quantification ( $NT_{50} = 80$ ) (Fig. 1C). In contrast,  
90 administration of a booster dose recovered the neutralizing antibody response against all Omicron  
91 subvariants (Fig. 1D, Fig. S1A-H). In serum from the boosted individuals, BA.2.75 exhibited 4.8-  
92 fold ( $p < 0.0001$ ) lower neutralization than D614G, with somewhat stronger neutralization  
93 resistance than BA.2 and BA.2.12.1, which were neutralized 3.6-fold ( $p < 0.01$ ) and 3.5-fold ( $p <$   
94  $0.001$ ) less efficiently than D614G, respectively (Fig. 1D). However, BA.2.75 showed higher  
95 neutralization sensitivity than BA.4/5, which had 9.7-fold ( $p < 0.001$ ) lower neutralization than  
96 D614G (Fig. 1D).

97 We also examined the neutralizing antibody response in a cohort of non-ICU COVID-19  
98 patients (n = 30) hospitalized at the Ohio State University Wexner Medical Center during the  
99 Omicron-wave of the pandemic. These patient samples were collected between early February  
100 and early March of 2022, representing a BA.1 dominant period in Ohio. Overall, the nAb titers of  
101 the Omicron-wave patients were much lower than those of boosted HCWs, and BA.2.75 exhibited  
102 neutralization resistance modestly higher than BA.2 (by 44.0%,  $p > 0.05$ ) but much lower than  
103 BA.4/5 (3.8-fold;  $p < 0.001$ ) relative to D614G (Fig. 1E; Fig. S1I). This cohort of Omicron-wave  
104 patients included 14 unvaccinated patients, 8 patients vaccinated with 2 doses of Moderna  
105 mRNA-1273 (n = 4) or Pfizer/BioNTech BNT162b2 (n = 4), and 8 patients vaccinated and boosted  
106 with Pfizer/BioNTech BNT162b2. We found that, while BA.2.75 was neutralized comparably to  
107 BA.2 and D614G for unvaccinated patients, BA.2.75 was neutralized 2.3-fold less efficiently than  
108 D614G in 2-dose vaccinated patients ( $p > 0.05$ ) and 4.9-fold less efficiently for 3-dose vaccinated  
109 patients ( $p < 0.01$ ), respectively (Fig. 1F). The boosted HCWs with breakthrough infection  
110 exhibited higher nAb titers overall (Fig. 1F), as would be expected.

111

112 *BA.2.75 neutralization is modulated by G446S, N460K, and R493Q mutations.*

113 To understand the determinants of BA.2.75 neutralization resistance, we examined all  
114 nine point mutations in the BA.2 background, as well as nine corresponding reversion mutations  
115 in the background of BA.2.75. None of these single mutations substantially impacted lentiviral  
116 pseudotype infectivity (Fig. 2A-B). We then examined the neutralization sensitivity of these  
117 mutants to sera from 9 HCWs collected 1-12 weeks after homologous booster vaccination with  
118 Moderna mRNA-1273 (n = 2) or Pfizer/BioNTech BNT162b2 (n = 7). When the G446S mutation  
119 was introduced to BA.2, a slight but significant reduction in sensitivity to 3-dose mRNA vaccine-  
120 induced nAbs was observed (42.7%,  $p < 0.01$ ), which was comparable to BA.2.75 (Fig. 2C).  
121 Introduction of a S446G reversion mutation into BA.2.75 enhanced neutralization sensitivity by  
122 31.4%, albeit the change was not statistically significant ( $p = 0.055$ ) (Fig. 2D). Interestingly,

123 introduction of a R493Q mutation into BA.2 increased neutralization sensitivity by 35.8% ( $p >$   
124 0.05), while introduction of the Q493R reversion mutation into BA.2.75 reduced neutralization  
125 sensitivity by 45.1% ( $p > 0.05$ ) (Fig. 2C-D). Of note, the N460K mutation also substantially  
126 increased neutralization resistance of BA.2 by 33.0% ( $p > 0.05$ ), whereas the K460N reversion  
127 mutation in BA.2.75 was 77.4% ( $p = 0.069$ ) more neutralization sensitive (Fig. 2C-D). Thus, the  
128 G446S and N460K mutations in BA.2.75 are largely responsible for its enhanced neutralization  
129 resistance, while the R493Q reversion mutation in BA.2.75 at least partially restores neutralizing  
130 epitopes found in the prototype SARS-CoV-2, which were otherwise abolished in BA.2.

131

132 *BA.2.75 exhibits enhanced syncytia formation and S processing compared to BA.2.*

133 We next sought to characterize key features of the BA.2.75 S protein, including the ability  
134 to mediate cell-cell fusion. HEK293T-ACE2 cells were transfected to express GFP and variant  
135 SARS-CoV-2 S proteins. As previously reported (Zeng et al., 2021), all Omicron sublineages  
136 exhibited reduced fusogenicity compared to the ancestral D614G S (Fig. 3A-B). However,  
137 BA.2.75 exhibited enhanced syncytia formation compared to BA.2, with mean syncytia size 2.0-  
138 fold higher than BA.2 ( $p < 0.0001$ ) (Fig. 3A-B; Fig. S2A); this was despite similar surface  
139 expression, as examined by flow cytometry (Fig. 3C-D).

140 To determine if the enhanced fusogenicity phenotype might be related to alterations in  
141 processing of S protein, we examined cell lysates from the pseudotyped lentivirus producer. As  
142 shown in Figure 3E, BA.2.75 spike exhibited enhanced processing, as reflected in the ratio of S1  
143 or S2 subunit to full length S ratio, which was ~30-40% higher than BA.2. Consistent with its  
144 enhanced fusion, BA.4/5 showed the highest S processing among omicron variants (Fig. 3A-B  
145 and E; Fig. S2A).

146

147 *Enhanced syncytia formation and processing of BA.2.75 is determined by the N460K mutation.*

148 We further characterized the impact of BA.2.75-defining mutations on S fusogenicity and  
149 processing. Introduction of the N460K mutation into the BA.2 S drastically enhanced cell-cell  
150 fusion, with mean syncytia size 3.8-fold ( $p < 0.0001$ ) higher than BA.2 (Fig. 4A-B; Fig. S2B).  
151 Conversely, introduction of the K460N reversion mutation into BA.2.75 significantly reduced cell-  
152 cell fusion, with mean syncytia size 4.3-fold ( $p < 0.0001$ ) lower than BA.2.75 (Fig. 4C-D; Fig. S2C).  
153 We found that F157L and G257S in the BA.2 background, as well as the R152W reversion mutant  
154 in the BA.2.75 background, also exhibited modestly altered fusion activity (Fig. 4A-D). Importantly,  
155 the differences in membrane fusion between these mutants were not due to the surface  
156 expression level of S, as examined by flow cytometry (Fig. 4E-F; Fig. S2D-E). Consistent with  
157 enhanced fusion activity, introduction of the N460K mutation into the BA.2 S protein enhanced  
158 processing of S into the S1 and S2 subunits, as reflected in a S1/S ratio 40% higher than in BA.2  
159 (Fig. 4G); a similar 70% increase in S2/S ratio was also observed (Fig. 4G). Conversely,  
160 introduction of a K460N reversion mutation into BA.2.75 reduced S protein processing by 20%  
161 (Fig. 4H). Thus, the N460K mutation in BA.2.75 enhances S processing, consistent with increased  
162 fusogenicity.

163

#### 164 *Structural modeling*

165 To understand how BA.2.75 mutations contribute to functional changes, we created  
166 models of BA.2.75 spike protein and its complex with the ACE2 receptor using homology  
167 modeling (Fig. 4I). The G446S mutation does not appear to alter main chain interactions with the  
168 Q42 receptor residue; however, this mutation could reduce backbone flexibility, thus potentially  
169 stabilizing the specific interaction with ACE2, as well as spike integrity. The R493Q mutation  
170 would abolish a strong salt-bridge interaction with the E35 residue on the ACE2 receptor, which  
171 could reduce receptor binding affinity; however, this effect may be offset by the formation two new  
172 hydrogen bonds between the Q493 residue on spike and residues E35 and K31 on ACE2. Finally,  
173 N460K forms a new hydrogen bond with the glycan-N90 on ACE2 through an elongated side

174 chain that reaches out to the alpha-1,3 mannose molecule on the N-linked glycan of the receptor  
175 residue N90, and this would likely enhance receptor binding affinity of BA.2.75.

176

## 177 **Discussion**

178         The BA.2.75 subvariant is the latest in a series of Omicron variants to be identified.  
179 BA.2.75 has an alarming nine additional S mutations compared with BA.2, and preliminary reports  
180 suggest a slight growth advantage (Callaway, 2022; World Health Organization, 2022). These  
181 features portend that BA.2.75 could potentially overtake the BA.4/5 subvariants as the dominant  
182 circulating strain. Given this concern, it is critical to examine key features and novel phenotypes  
183 of BA.2.75, especially in its S protein. In this study, we show that BA.2.75 exhibits an increased  
184 neutralization resistance compared to ancestral BA.2, but has significantly lower neutralization  
185 resistance than BA.4/5 for 3-dose mRNA vaccinated HCWs as well as for hospitalized Omicron-  
186 wave patients. Critically, we demonstrate that the G446S and N460K mutations in the S protein  
187 of BA.2.75 underlie its enhanced neutralization resistance, while the R493Q mutation in BA.2.75,  
188 which is a reversion mutation, sensitizes it to neutralization. These findings could reflect the  
189 emergence of compensatory mutations to improve S function while maintaining neutralization  
190 resistance. Notably, the G446S mutation occurs in an epitope bound by class III neutralizing  
191 antibodies, rather than class II neutralizing antibodies that target the epitope of the R493Q  
192 mutation (Greaney et al., 2021). Structural analysis suggests that the side chain addition by  
193 G446S creates a steric clash with the CDR region of class III neutralizing antibodies, thus  
194 potentially hampering their recognition (Liu et al., 2022; Wang et al., 2022a). Hence, the exchange  
195 of these mutations may alter the susceptibility of BA.2.75 to class II and class III nAbs.

196         We further demonstrate that BA.2.75 exhibits enhanced S-mediated cell-cell fusion  
197 compared to BA.2, albeit to a lesser extent than BA.4/5. This enhanced triggering of BA.2.75 S-  
198 mediated fusion may reflect improved receptor utilization that is not present in earlier Omicron  
199 subvariants, consistent with several recent preprints (Cao et al., 2022; Saito et al., 2022; Wang



200 et al., 2022a). Critically, we find that the N460K mutation present in BA.2.75 is essential for the  
201 enhanced fusion phenotype. This may relate to enhanced processing of N460K-containing S in  
202 virus producing cells, which would prime more cell surface-associated S for membrane fusion.  
203 While structural modeling did not provide an immediate explanation, the N460K mutation might  
204 enhance receptor utilization through a hydrogen bond with the receptor glycan N90. However, it  
205 is worth noting that this glycan interaction is mediated by a terminal mannose molecule, so it may  
206 not be easily observed in conditions of protein overexpression where glycosylation is often  
207 insufficient. G446S, on the other hand, may reduce the flexibility of loop 440-450, potentially  
208 enhancing overall spike thermostability, which likely decreases S processing efficiency.  
209 Furthermore, G446 is not well resolved in many apo spike structures, in line with its flexible local  
210 conformation. A more stable backbone loop conformation produced by the G446S mutation may  
211 reduce the energy cost for receptor engagement through hydrogen bond formation with Q42.  
212 Lastly, the loss of a strong salt-bridge interaction by the R493Q mutation is offset by the addition  
213 of two potential hydrogen bonds to the adjacent receptor residues, which could explain its  
214 modestly decreased fusion efficiency and processing. The contributions of these key residues to  
215 BA.2.75 replication kinetics in physiologically relevant human lung and airway epithelial cells  
216 needs to be carefully investigated. Further characterization of emerging SARS-CoV-2 variants will  
217 continue to aid our understanding of key features of SARS-CoV-2 evolution, spike biology, and  
218 immune evasion. Continued analysis of emerging variants also will improve ongoing public health  
219 responses and any potential reformulation of SARS-CoV-2 mRNA vaccine boosters.

220         Limitations of this study include a relatively small sample size for the boosted health care  
221 workers and the utilization of pseudotyped lentivirus for the neutralization assay rather than an  
222 authentic virus assay. However, our results for neutralization resistance are in accordance with  
223 several recent preprints (Cao et al., 2022; Gruell et al., 2022; Saito et al., 2022; Sheward et al.,  
224 2022; Wang et al., 2022b; Xie et al., 2022; Yamasoba et al., 2022a). Additionally, the lentiviral  
225 pseudotype neutralization assay has been previously validated by assays with authentic SARS-

226 CoV-2 (Zeng et al., 2020), and confirmed by numerous laboratories in the field. Future studies  
227 will focus on the biology and replication characteristics of BA.2.75 using variants isolated from  
228 human COVID patients.

229

### 230 **Author Contributions**

231 S.-L.L. conceived and directed the project. P.Q. performed most of the experiments. J.P.E.  
232 assisted in experiments and contributed data processing and analyses. C.C. and R.J.G. provided  
233 clinical samples. P.Q., J.P.E., and S.-L.L. wrote the paper. K.X. performed homology modeling.  
234 Y.-M.Z, L.J.S., E.M.O. and K.X. provided insightful discussion and revision of the manuscript.

235

### 236 **Acknowledgements**

237 We thank the NIH AIDS Reagent Program and BEI Resources for providing important reagents  
238 for this work and Xue Zou for assistance. We also thank the Clinical Research Center/Center for  
239 Clinical Research Management of The Ohio State University Wexner Medical Center and The  
240 Ohio State University College of Medicine in Columbus, Ohio, specifically Francesca Madiai, Dina  
241 McGowan, Breona Edwards, Evan Long, and Trina Wemlinger, for logistics, collection and  
242 processing of samples. In addition, we thank Sarah Karow, Madison So, Preston So, Daniela  
243 Farkas, and Finny Johns in the clinical trials team of The Ohio State University for sample  
244 collection and other supports.

245

### 246 **Funding**

247 This work was supported by a fund provided by an anonymous private donor to OSU. S.-L.L.,  
248 R.J.G., L.J.S. and E.M.O. were supported by the National Cancer Institute of the NIH under award  
249 no. U54CA260582. The content is solely the responsibility of the authors and does not necessarily  
250 represent the official views of the National Institutes of Health. J.P.E. was supported by Glenn  
251 Barber Fellowship from the Ohio State University College of Veterinary Medicine. R.J.G. was

252 additionally supported by the Robert J. Anthony Fund for Cardiovascular Research and the JB  
253 Cardiovascular Research Fund, and L.J.S. was partially supported by NIH R01 HD095881. K.X.  
254 was supported by Path to K Grant through the Ohio State University Center for Clinical &  
255 Translational Science.

256

## 257 **Declaration of Interests**

258 The authors declare no competing interests.

259

## 260 **Figure Legends:**

261 **Figure 1: BA.2.75 exhibits strong neutralization resistance to 2-dose and 3-dose mRNA**  
262 **vaccinee sera and Omicron wave patient sera. (A)** Schematic of BA.2-derived SARS-CoV-2  
263 variants with mutations relative to the BA.2 background indicated. Highlighted are the S1 and S2  
264 subunits, N-terminal domain (NTD), receptor binding domain (RBD), fusion peptide (FP), and  
265 transmembrane domain (TM). **(B)** Infectivity of pseudotyped lentivirus bearing S protein from  
266 SARS-CoV-2 variants of study; bars represent means  $\pm$  standard error. **(C-D)** Neutralizing  
267 antibody titers against lentivirus pseudotyped with S from individual SARS-CoV-2 variants for 15  
268 health care workers for sera collected 3-4 weeks after second mRNA vaccination (C) or 1-12  
269 weeks after homologous mRNA booster vaccination (D). **(E)** Neutralizing antibody titers for sera  
270 collected from 30 COVID-19 patients hospitalized during the BA.1 pandemic wave. **(F)**  
271 Neutralizing antibody titers against hospitalized BA.1 wave patients are divided by vaccination  
272 status. (C-F) Dots indicate individual patient samples; bars represent geometric means with 95%  
273 confidence intervals; significance relative to D614G was determined by one-way repeated  
274 measures ANOVA with Bonferroni multiplicity correction. P-values are displayed as \* $p < 0.05$ , \*\* $p$   
275  $< 0.01$ , \*\*\* $p < 0.001$ , \*\*\*\* $p < 0.0001$ , and ns for not significant.

276

277 **Figure 2: The G446S, N460K, and R493Q mutations modulate BA.2.75 neutralization**  
278 **sensitivity. (A)** Relative infectivity of lentivirus pseudotyped with BA.2 S with single mutations  
279 from BA.2.75 lineage defining mutations; bars represent means  $\pm$  standard error. **(B)** Relative  
280 infectivity of lentivirus pseudotyped with BA.2.75 S with single reversion mutations to remove  
281 BA.2.75 lineage defining mutations; bars represent means  $\pm$  standard error. **(C-D)** Neutralizing  
282 antibody titers against lentivirus pseudotyped with S from BA.2 with single mutations from BA.2.75  
283 lineage-defining mutations (C) or BA.2.75 with single reversion mutations from BA.2.75 lineage-  
284 defining mutations (D) for sera collected from 9 health care workers 1-12 weeks after homologous  
285 mRNA booster vaccination. Dots indicate individual patient samples; bars represent geometric  
286 means with 95% confidence intervals; significance relative to D614G was determined by one-way  
287 repeated measures ANOVA with Bonferroni multiplicity correction. P-values are displayed as \*\*p  
288 < 0.01, and ns for not significant.

289  
290 **Figure 3: BA.2.75 exhibits enhanced cell-cell fusion and S processing. (A)** Fluorescence  
291 images displaying syncytia formation are presented for HEK293T-ACE2 cells 48 hr after co-  
292 transfection with a GFP expression construct and SARS-CoV-2 variant S proteins. **(B)**  
293 Quantification of syncytia formation in panel (A) displays the mean syncytia size; bars represent  
294 means  $\pm$  standard error, with significance relative to D614G determined by one-way ANOVA with  
295 Bonferroni multiplicity correction. **(C)** Histogram displays of the surface staining of HEK293T cells  
296 expressing S proteins, which were detected by an anti-S1 antibody (T62). **(D)** Quantification of  
297 relative surface expression as shown in (C); bars represent means  $\pm$  standard error. **(E)**  
298 Pseudotyped lentivirus producer cell lysate was assessed for processing of S by probing with  
299 anti-S1 (T62), anti-S2, anti-HIV-1 Gag (anti-p24), and anti-GAPDH. Band intensities were  
300 quantified in ImageJ and the ratio of S1/S or S2/S is displayed relative to the S1/S or S2/S ratio  
301 of BA.2. P-values are displayed as \*\*\*\*p < 0.0001.

302

303 **Figure 4: The N460K mutation determines enhanced cell-cell fusion and S processing of**  
304 **BA.2.75.** (A) Fluorescence images displaying syncytia formation are presented for HEK293T-  
305 ACE2 cells 48 hr after co-transfection with a GFP expression construct and BA.2 single mutant S  
306 proteins. (B) Quantification of syncytia formation in panel (A) displays the mean syncytia size;  
307 bars represent means  $\pm$  standard error, with significance relative to D614G determined by one-  
308 way ANOVA with Bonferroni multiplicity correction. (C) Fluorescence images displaying syncytia  
309 formation are presented for HEK293T-ACE2 cells 48-hrs after co-transfection with a GFP  
310 expression construct and BA.2.75 single reversion mutant S proteins. (D) Quantification of  
311 syncytia formation in panel (C) displays the mean syncytia size; bars represent means  $\pm$  standard  
312 error, with significance relative to D614G determined by one-way ANOVA with Bonferroni  
313 multiplicity correction. (E-F) Quantification of relative S surface expression in transfected  
314 HEK293T cells for BA.2 single mutants (E) or BA.2.75 reversion mutants (F), as examined by flow  
315 cytometry; bars represent means  $\pm$  standard error. (G) Pseudotyped lentivirus producer cell lysate  
316 was assessed for processing of S from BA.2 single mutants by probing with anti-S1 (T62), anti-  
317 S2, anti-HIV-1 p24, and anti-GAPDH. Band intensities were quantified in ImageJ and the ratios  
318 of S1/S and S2/S are displayed relative to the S1/S and S2/S ratios of BA.2. (H) Pseudotyped  
319 lentivirus producer cell lysate was assessed for processing of S from BA.2.75 reversion mutants  
320 by probing with anti-S1, anti-S2, anti-HIV-1 p24, and anti-GAPDH. Band intensities were  
321 quantified in ImageJ and the ratios of S1/S and S2/S are displayed relative to the S1/S and S2/S  
322 ratios of BA.2.75. (I) Structural modelling of Omicron BA.2.75 spike protein viewed as a ribbon.  
323 Mutations of BA.2.75 specific mutants are highlighted by red spheres. The RBD of the cyan spike  
324 protomer is in an “up” conformation. Upper inset: The mutation G446S reduces the backbone  
325 flexibility and possibly stabilizes the hydrogen bond between its carbonyl group and the residue  
326 Q42 on ACE2 receptor (green); the mutation R493Q abolishes the salt-bridge interaction with the  
327 E35 on ACE2 receptor and potentially forms two hydrogen bonds with E35 and K31. Lower inset:  
328 the mutation N460K enables formation of a hydrogen bond with the glycan-N90 on ACE2 receptor

329 (green). In all cases, p-values are displayed as \* $p < 0.05$ , \*\* $p < 0.01$ , \*\*\*\* $p < 0.0001$ , and ns for  
330 not significant.

331  
332 **Figure S1: Neutralization of Omicron subvariants by vaccinee and COVID-19 patient sera,**  
333 **related to Figure 1. (A-F)** Comparison of the neutralizing antibody titers in HCWs between 2-  
334 dose and 3-dose booster mRNA vaccination against the D614G (A), BA.1 (B), BA.2 (C), BA.2.12.1  
335 (D), BA.4/5 (E), and BA.2.75 (F) variants. Lines connect samples from the same HCW, the dotted  
336 lines represent the limit of quantification ( $NT_{50} = 80$ ), and significance was determined by paired,  
337 two-tailed Student's t test with Welch's correction. **(G-I)** Heatmaps display the nAb titers for HCWs  
338 3-4 weeks after second mRNA vaccine dose (G), 1-12 weeks after mRNA vaccine booster dose  
339 (H), and for hospitalized Omicron wave COVID-19 patients (I). HCWs are indicated as 'M' for  
340 Moderna mRNA-1273 vaccinated or 'P' for Pfizer/BioNTech BNT162b2 vaccinated, and Omicron  
341 wave patients are indicated as 'U' for unvaccinated, 'V' for 2-dose vaccinated, and 'B' for  
342 vaccinated and boosted. P-values are represented as \*\* $p < 0.01$  and \*\*\*\* $p < 0.0001$ .

343  
344 **Figure S2: Syncytia formation and cell surface expression of Omicron subvariants, as well**  
345 **as BA.2- and BA.2.75-derived single mutants, related to Figures 3 and 4. (A-C)** Fluorescence  
346 images displaying syncytia formation are presented for HEK293T-ACE2 cells 24 hr after co-  
347 transfection with a GFP expression construct and SARS-CoV-2 variant S proteins (A), BA.2 single  
348 mutants S proteins (B), or BA.2.75 single reversion mutant S proteins (C). **(D-E)** Histograms of  
349 surface staining with anti-S1 antibody of HEK293T cells expressing S proteins from BA.2 with  
350 single mutations from BA.2.75 lineage defining mutations (D) and from BA.2.75 with single  
351 reversion mutations from BA.2.75 lineage defining mutations (E).

352

353 **STAR Methods**

354 **RESOURCE AVAILABILITY**

355 *Lead Contact*

356 Further information and requests for resources and reagents should be directed to the lead  
357 contact, Dr. Shan-Lu Liu ([liu.6244@osu.edu](mailto:liu.6244@osu.edu)).

358

359 *Materials Availability*

360 Plasmids generated in this study are available upon request made to the lead contact.

361

362 *Data and Code Availability*

- 363
- NT<sub>50</sub> values and de-identified patient information will be deposited to the National Cancer  
364 Institute SeroNet Coordinating Center. Additionally, NT<sub>50</sub> values and de-identified patient  
365 information reported in this paper will be shared by the lead contact upon request.
  - This paper does not report original code.
  - Any additional information required to reanalyze the data reported in this paper is available  
368 from the lead contact upon request.

369

370 EXPERIMENTAL MODEL AND SUBJECT DETAILS

371 *Patient Information*

372 Sera were collected from the Ohio State University Wexner Medical Center health care  
373 workers (HCWs) under approved IRB protocols (2020H0228 and 2020H0527). Demographic  
374 information was self-reported and all subjects provided informed consent. Sera from 15 HCWs  
375 were collected 3-4 weeks after vaccination with a second dose of Moderna mRNA-1273 (n = 7)  
376 or Pfizer/BioNTech BNT162b2 (n = 8) vaccine, and 1-12 weeks after vaccination with a  
377 homologous booster dose. These HCWs ranged in age from 32 to 56 years (median 37 years)  
378 and included 6 female and 9 male HCWs. Analysis by age and gender could not be performed  
379 due to low sample number.

380 Sera were collected from patients 30 hospitalized for COVID-19 at the Ohio State  
381 University Wexner Medical Center under an approved IRB protocol (2020H0527). Sera were  
382 collected between early February and early March of 2022, during the Omicron wave in Ohio.  
383 Patients included 14 unvaccinated patients, 8 patients vaccinated with 2 doses of Moderna  
384 mRNA-1273 (n = 4) or Pfizer/BioNTech BNT162b2 (n = 4), and 8 patients vaccinated and boosted  
385 with Pfizer/BioNTech BNT162b2. This cohort included 11 female and 19 male patients. Patients  
386 ranged in age from 28 to 78 years (median 62 years).

387

### 388 *Cell Lines and Maintenance*

389 HEK293T (ATCC CRL-11268, RRID: CVCL\_1926) and HEK293T-ACE2 (BEI NR-52511,  
390 RRID: CVCL\_A7UK) cells were maintained in Dulbecco's Modified Eagle's Medium (DMEM)  
391 (Cibco, 11965-092) supplemented with 10% Fetal Bovine Serum (Signa, F1051) and 1%  
392 penicillin/streptomycin (HyCline, SV30010). Cells were maintained at 5% CO<sub>2</sub> and 37°C.

393

## 394 METHOD DETAILS

### 395 *Plasmids*

396 Pseudotyped lentivirus was produced using a pNL4-3-inGluc lentivirus vector comprised  
397 of a ΔEnv HIV-1 backbone bearing a *Gaussia* luciferase reporter gene driven by a CMV promoter  
398 (Goerke et al., 2008; Zeng et al., 2020). SARS-CoV-2 S constructs bearing N- and C-terminal  
399 Flag tags were synthesized and cloned into a pcDNA3.1 vector by GenScript (Piscataway, NJ)  
400 by Kpn I and BamH I restriction enzyme cloning.

401

### 402 *Pseudotyped lentivirus production and infectivity*

403 Pseudotyped lentivirus was produced by transfecting HEK293T cells with pNL4-3-inGluc  
404 and S construct in a 2:1 ratio using polyethylenimine transfection. Pseudotyped lentivirus was  
405 collected at 48 hr and 72 hr after transfection. Collections were pooled and used to infect



406 HEK293T-ACE2 cells to assess pseudotyped lentivirus infectivity. 48 hr and 72 hr after infection,  
407 infected cell culture media was assessed for *Gaussia* luciferase activity by combining 20  $\mu$ L of  
408 media with 20  $\mu$ L of *Gaussia* luciferase substrate (0.1 M Tris pH 7.4, 0.3 M sodium ascorbate, 10  
409  $\mu$ M coelenterazine). Luminescence was then immediately measured by a BioTek Cytation5 plate  
410 reader using BioTek Gen5 Microplate Reader and Imager Software (Winooski, VT).

411

#### 412 *Lentivirus neutralization assay*

413 Pseudotyped lentivirus neutralization assays were performed as previously described  
414 (Zeng et al., 2020). Patient or HCW sera were 4-fold serially diluted in complete DMEM and  
415 pseudotyped lentivirus was added to neutralize for 1 hr (final dilutions: 1:80, 1:320, 1:1280, 1:5120,  
416 1:20480, and no serum control). The pseudotyped lentivirus/sera mixtures were then transferred  
417 to HEK293T-ACE2 cells for infection. Then 48 hr and 72 hr after infection, infected cell media was  
418 assayed for *Gaussia* luciferase activity by combining 20  $\mu$ L of cell culture media with 20  $\mu$ L of  
419 *Gaussia* luciferase substrate. Luminescence was read immediately by a BioTek Cytation5 plate  
420 reader using BioTek Gen5 Microplate Reader and Imager Software (Winooski, VT). NT<sub>50</sub> values  
421 were determined by least-squares-fit, non-linear regression in GraphPad Prism 9 (San Diego,  
422 CA).

423

#### 424 *Spike surface expression*

425 HEK293T cells used to produce pseudotyped lentivirus were singularized by incubation in  
426 phosphate buffer saline (PBS) with 5 mM ethylenediaminetetraacetic acid (EDTA) at 37°C for 5  
427 min and fixed 72 hr after transfection by incubation in 3.7% formaldehyde in PBS for 10 min. Cells  
428 were then stained with rabbit anti-S1 primary antibody (Sino Biological, 40150-T62) and anti-  
429 rabbit-IgG-FITC secondary antibody (Sigma, F9887). Samples were analyzed by a Life  
430 Technologies Attune NxT flow cytometer and data was processed using FlowJo v7.6.5 (Ashland,  
431 OR).

432

433 *Syncytia formation*

434 HEK293T-ACE2 cells were transfected with SARS-CoV-2 S constructs and a GFP  
435 expression construct. Cells were then imaged at 4x magnification 24 hr and 48 hr after transfection  
436 with a Leica DMI8 confocal microscope. Syncytia size was quantified using Leica Applications  
437 Suit X (Wetzlar, Germany) image analysis software. Three images were taken per sample with  
438 representative images being displayed.

439

440 *Spike processing and incorporation*

441 Pseudotyped lentivirus producing HEK293T cells were lysed by incubating in RIPA lysis  
442 buffer (50 mM Tris pH 7.5, 150 mM NaCl, 1mM EDTA, Nonidet P-40, 0.1% sodium dodecyl sulfate  
443 (SDS)) supplemented with protease inhibitor (Sigma, P8340) on ice for 30 min. Cell debris was  
444 pelleted and cell lysate was dissolved in 5x SDS-PAGE Laemmli buffer (312.5 mM Tris-HCl pH  
445 6.8, 10% SDS, 25% glycerol, 0.5% Bromophenol blue, 10%  $\beta$ -mercaptoethanol). Pseudotyped  
446 lentivirus was purified by ultracentrifugation through a 20% sucrose cushion at 28,000 rpm and  
447 4°C using a Beckman L-80 ultracentrifuge with TW-41 rotor. Pelleted pseudotyped lentivirus was  
448 resuspended in 1x SDS-PAGE Laemmli buffer. Cell lysate and purified virus were run on a 10%  
449 acrylamide SDS-PAGE gel and were transferred to a PVDF membrane. Membranes were blotted  
450 with anti-S1 (Sino Biological, 40150-T62), anti-S2 (Sino Biological, 40590-T62), anti-p24 (NIH  
451 ARP-1513), and anti-GAPDH (Santa Cruz Biotech, sc-47724) with anti-mouse-IgG-peroxidase  
452 (Sigma A5278) and anti-rabbit-IgG-HRP (Sigma, A9169) secondary antibodies. Blots were  
453 imaged with Immobilon Crescendo Western HRP substrate (Millipore, WBLUR0500) on a GE  
454 Amersham Imager 600. Band intensities were quantified using ImageJ (Bethesda, MD) image  
455 analysis software.

456

457 *Homology modeling*

458 Structural modeling of Omicron BA.2.75 spike protein and its complex with ACE2 receptor was  
459 conducted on SWISS-MODEL server with cryo-EM structure of SARS-CoV2 Omicron BA2 strain  
460 spike and complexes (PDB 7TNW and 7XB0) as templates. Glycan modeling, residue  
461 examination and rotamer adjustment were carried out manually with programs Coot (Cambridge,  
462 England) and PyMOL (New York, NY).

463

#### 464 *Quantification and statistical analysis*

465 NT<sub>50</sub> values were determined by least-squares-fit, non-linear-regression in GraphPad  
466 Prism 9 (San Diego, CA). NT<sub>50</sub> values were log<sub>10</sub> transformed for hypothesis testing to better  
467 approximate normality. Throughout, multiplicity was addressed by the use of Bonferroni  
468 corrections. Statistical analyses were performed using GraphPad Prism 9 (San Diego, CA) and  
469 are referenced in the figure legends and include one-way ANOVA (Fig. 3B and Fig. 4B and D),  
470 one-way repeated measures ANOVA (Fig. 1C-F, Fig. 2C-D), and a paired, two-tailed Student's t  
471 test with Welch's correction was used (Fig. S1A-F). Syncytia sizes were quantified by Leica  
472 Applications Suit X (Wetzlar, Germany). Band intensities (Figs. 3E and Fig. 4G-H) were quantified  
473 by ImageJ (Bethesda, MD) image analysis software.

474

#### 475 **References:**

- 476 Callaway, E. 2022. Will 'Centaurus' be the next global coronavirus variant? Indian cases offer  
477 clues. *Nature*.
- 478 Cao, Y., W. Song, L. Wang, P. Liu, C. Yue, F. Jian, Y. Yu, A. Yisimayi, P. Wang, Y. Wang, Q.  
479 Zhu, J. Deng, W. Fu, L. Yu, N. Zhang, J. Wang, T. Xiao, R. An, J. Wang, L. Liu, S. Yang,  
480 X. Niu, Q. Gu, F. Shao, X. Hao, R. Jin, Y. Wang, X.S. Xie, and X. Wang. 2022.  
481 Characterizations of enhanced infectivity and antibody evasion of Omicron BA.2.75.  
482 *bioRxiv*:2022.2007.2018.500332.
- 483 Centers for Disease Control and Prevention. 2022. COVID Data Tracker. Atlanta, GA: US  
484 Department of Health and Human Services, CDC. 2022, August 10.  
485 <https://covid.cdc.gov/covid-data-tracker>
- 486 Evans, J.P., C. Zeng, P. Qu, J. Faraone, Y.M. Zheng, C. Carlin, J.S. Bednash, T. Zhou, G.  
487 Lozanski, R. Mallampalli, L.J. Saif, E.M. Oltz, P.J. Mohler, K. Xu, R.J. Gumina, and S.L.  
488 Liu. 2022. Neutralization of SARS-CoV-2 Omicron sub-lineages BA.1, BA.1.1, and BA.2.  
489 *Cell Host Microbe*. 30:1093-1102.e1093.

- 490 Goerke, A.R., A.M. Loening, S.S. Gambhir, and J.R. Swartz. 2008. Cell-free metabolic  
491 engineering promotes high-level production of bioactive *Gaussia princeps* luciferase.  
492 *Metab Eng.* 10:187-200.
- 493 Greaney, A.J., T.N. Starr, C.O. Barnes, Y. Weisblum, F. Schmidt, M. Caskey, C. Gaebler, A. Cho,  
494 M. Agudelo, S. Finkin, Z. Wang, D. Poston, F. Muecksch, T. Hatzioannou, P.D. Bieniasz,  
495 D.F. Robbani, M.C. Nussenzweig, P.J. Bjorkman, and J.D. Bloom. 2021. Mapping  
496 mutations to the SARS-CoV-2 RBD that escape binding by different classes of antibodies.  
497 *Nat Commun.* 12:4196.
- 498 Gruell, H., K. Vanshylla, P. Tober-Lau, D. Hillus, P. Schommers, C. Lehmann, F. Kurth, L.E.  
499 Sander, and F. Klein. 2022. mRNA booster immunization elicits potent neutralizing serum  
500 activity against the SARS-CoV-2 Omicron variant. *Nat Med.* 28:477-480.
- 501 Hoffmann, M., N. Krüger, S. Schulz, A. Cossmann, C. Rocha, A. Kempf, I. Nehlmeier, L. Graichen,  
502 A.S. Moldenhauer, M.S. Winkler, M. Lier, A. Dopfer-Jablonka, H.M. Jäck, G.M.N. Behrens,  
503 and S. Pöhlmann. 2022. The Omicron variant is highly resistant against antibody-mediated  
504 neutralization: Implications for control of the COVID-19 pandemic. *Cell.* 185:447-456.e411.
- 505 Liu, L., S. Iketani, Y. Guo, J.F. Chan, M. Wang, L. Liu, Y. Luo, H. Chu, Y. Huang, M.S. Nair, J.  
506 Yu, K.K. Chik, T.T. Yuen, C. Yoon, K.K. To, H. Chen, M.T. Yin, M.E. Sobieszczyk, Y.  
507 Huang, H.H. Wang, Z. Sheng, K.Y. Yuen, and D.D. Ho. 2022. Striking antibody evasion  
508 manifested by the Omicron variant of SARS-CoV-2. *Nature.* 602:676-681.
- 509 Qu, P., J. Faraone, J.P. Evans, X. Zou, Y.M. Zheng, C. Carlin, J.S. Bednash, G. Lozanski, R.K.  
510 Mallampalli, L.J. Saif, E.M. Oltz, P.J. Mohler, R.J. Gumina, and S.L. Liu. 2022.  
511 Neutralization of the SARS-CoV-2 Omicron BA.4/5 and BA.2.12.1 Subvariants. *The New*  
512 *England Journal of Medicine.* 386:2526-2528.
- 513 Saito, A., T. Tamura, J. Zahradnik, S. Deguchi, K. Tabata, I. Kimura, J. Ito, H. Nasser, M. Toyoda,  
514 K. Nagata, K. Uriu, Y. Kosugi, S. Fujita, D. Yamasoba, M. Shofa, M.M. Begum, Y. Oda, R.  
515 Suzuki, H. Ito, N. Nao, L. Wang, M. Tsuda, K. Yoshimatsu, Y. Yamamoto, T. Nagamoto,  
516 H. Asakura, M. Nagashima, K. Sadamasu, K. Yoshimura, T. Ueno, G. Schreiber, A.  
517 Takaori-Kondo, K. Shirakawa, H. Sawa, T. Irie, K. Takayama, K. Matsuno, S. Tanaka, T.  
518 Ikeda, T. Fukuhara, and K. Sato. 2022. Virological characteristics of the SARS-CoV-2  
519 Omicron BA.2.75. *bioRxiv:2022.2008.2007.503115*.
- 520 Sheward, D.J., C. Kim, J. Fischbach, S. Muschiol, R.A. Ehling, N.K. Björkström, G.B. Karlsson  
521 Hedestam, S.T. Reddy, J. Albert, T.P. Peacock, and B. Murrell. 2022. Evasion of  
522 neutralizing antibodies by Omicron sublineage BA.2.75. *bioRxiv:2022.2007.2019.500716*.
- 523 Tuekprakhon, A., R. Nutalai, A. Dijokaite-Guraliuc, D. Zhou, H.M. Ginn, M. Selvaraj, C. Liu, A.J.  
524 Mentzer, P. Supasa, H.M.E. Duyvesteyn, R. Das, D. Skelly, T.G. Ritter, A. Amini, S. Bibi,  
525 S. Adele, S.A. Johnson, B. Constantinides, H. Webster, N. Temperton, P. Klenerman, E.  
526 Barnes, S.J. Dunachie, D. Crook, A.J. Pollard, T. Lambe, P. Goulder, N.G. Paterson, M.A.  
527 Williams, D.R. Hall, E.E. Fry, J. Huo, J. Mongkolsapaya, J. Ren, D.I. Stuart, and G.R.  
528 Screaton. 2022. Antibody escape of SARS-CoV-2 Omicron BA.4 and BA.5 from vaccine  
529 and BA.1 serum. *Cell.* 185:2422-2433.e2413.
- 530 Wang, Q., S. Iketani, Z. Li, Y. Guo, A.Y. Yeh, M. Liu, J. Yu, Z. Sheng, Y. Huang, L. Liu, and D.D.  
531 Ho. 2022a. Antigenic characterization of the SARS-CoV-2 Omicron subvariant BA. 2.75.  
532 *bioRxiv*.
- 533 Wang, X., J. Ai, X. Li, X. Zhao, J. Wu, H. Zhang, X. He, C. Zhao, R. Qiao, M. Li, Y. Cui, Y. Chen,  
534 L. Yang, Z. Hu, C. Xu, W. Zhang, and P. Wang. 2022b. Neutralization of Omicron  
535 BA.4/BA.5 and BA.2.75 by Booster Vaccination or BA.2 Breakthrough Infection Sera.  
536 *bioRxiv:2022.2008.2004.502716*.
- 537 World Health Organization. 2022. Tracking SARS-CoV-2 variants. World Health Organization.  
538 2022, August 10. <https://www.who.int/en/activities/tracking-SARS-CoV-2-variants>.
- 539 Xie, X., J. Zou, C. Kurhade, M. Liu, P. Ren, and P.-Y. Shi. 2022. Neutralization of SARS-CoV-2  
540 Omicron sublineages by 4 doses of mRNA vaccine. *bioRxiv:2022.2007.2029.502055*.

- 541 Yamasoba, D., I. Kimura, Y. Kosugi, K. Uriu, S. Fujita, J. Ito, and K. Sato. 2022a. Neutralization  
542 sensitivity of Omicron BA.2.75 to therapeutic monoclonal antibodies.  
543 *bioRxiv:2022.2007.2014.500041*.
- 544 Yamasoba, D., I. Kimura, H. Nasser, Y. Morioka, N. Nao, J. Ito, K. Uriu, M. Tsuda, J. Zahradnik,  
545 K. Shirakawa, R. Suzuki, M. Kishimoto, Y. Kosugi, K. Kobiyama, T. Hara, M. Toyoda, Y.L.  
546 Tanaka, E.P. Butlertanaka, R. Shimizu, H. Ito, L. Wang, Y. Oda, Y. Orba, M. Sasaki, K.  
547 Nagata, K. Yoshimatsu, H. Asakura, M. Nagashima, K. Sadamasu, K. Yoshimura, J.  
548 Kuramochi, M. Seki, R. Fujiki, A. Kaneda, T. Shimada, T.A. Nakada, S. Sakao, T. Suzuki,  
549 T. Ueno, A. Takaori-Kondo, K.J. Ishii, G. Schreiber, H. Sawa, A. Saito, T. Irie, S. Tanaka,  
550 K. Matsuno, T. Fukuhara, T. Ikeda, and K. Sato. 2022b. Virological characteristics of the  
551 SARS-CoV-2 Omicron BA.2 spike. *Cell*. 185:2103-2115.e2119.
- 552 Zeng, C., J.P. Evans, R. Pearson, P. Qu, Y.M. Zheng, R.T. Robinson, L. Hall-Stoodley, J. Yount,  
553 S. Pannu, R.K. Mallampalli, L. Saif, E. Oltz, G. Lozanski, and S.L. Liu. 2020. Neutralizing  
554 antibody against SARS-CoV-2 spike in COVID-19 patients, health care workers, and  
555 convalescent plasma donors. *JCI Insight*. 5.
- 556 Zeng, C., J.P. Evans, P. Qu, J. Faraone, Y.M. Zheng, C. Carlin, J.S. Bednash, T. Zhou, G.  
557 Lozanski, R. Mallampalli, L.J. Saif, E.M. Oltz, P. Mohler, K. Xu, R.J. Gumina, and S.L. Liu.  
558 2021. Neutralization and Stability of SARS-CoV-2 Omicron Variant. *bioRxiv*.  
559

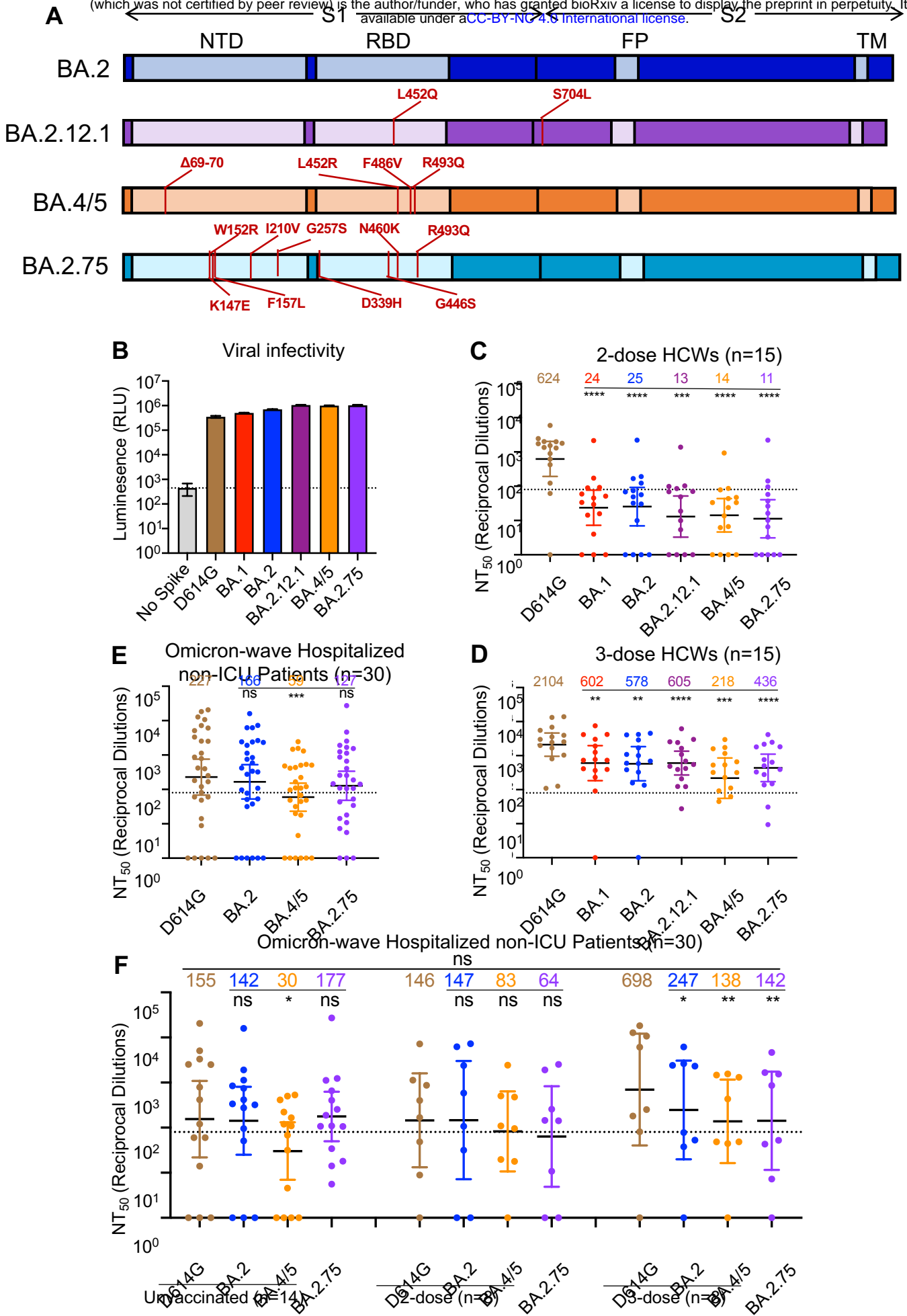


Figure 1

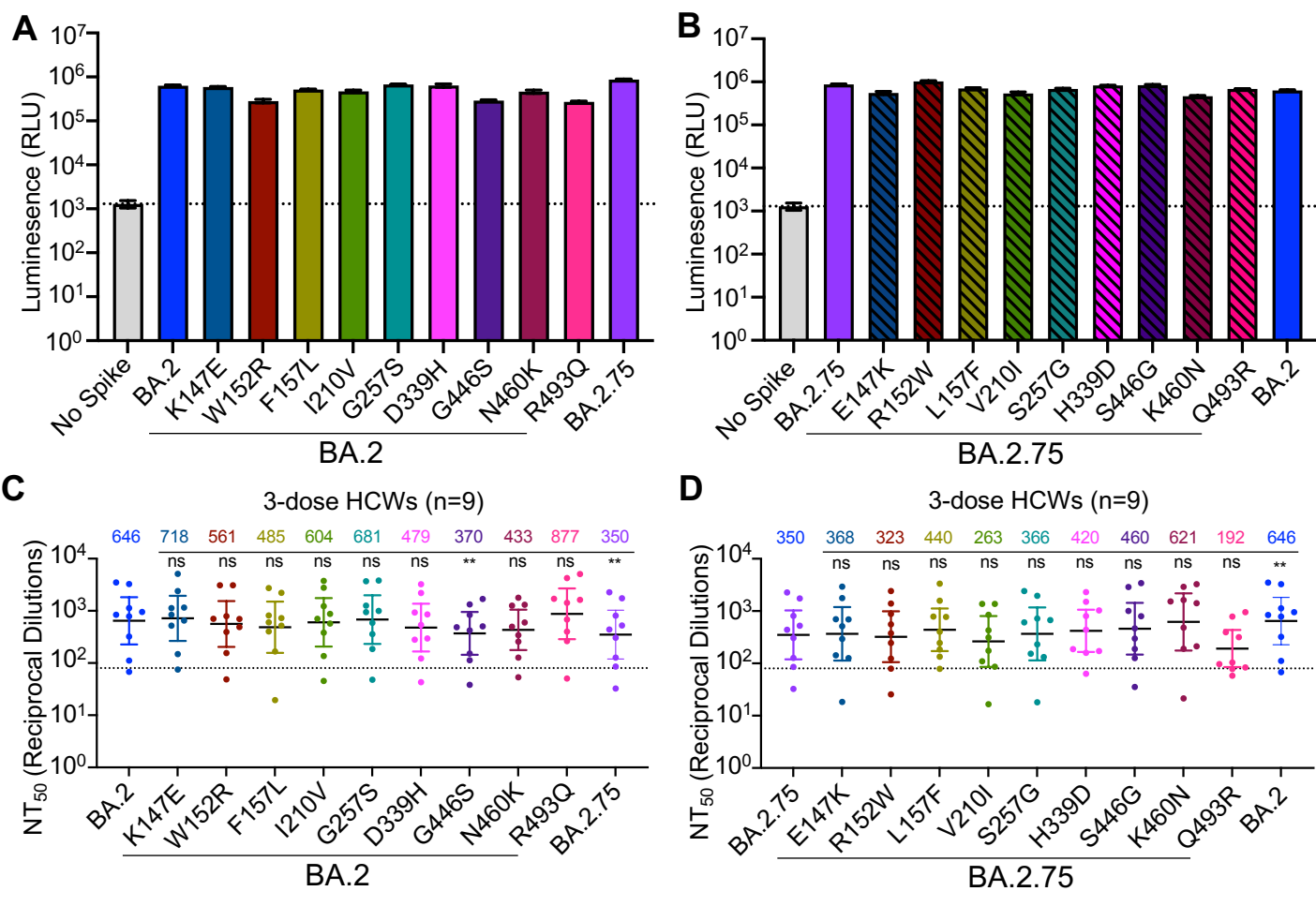


Figure 2

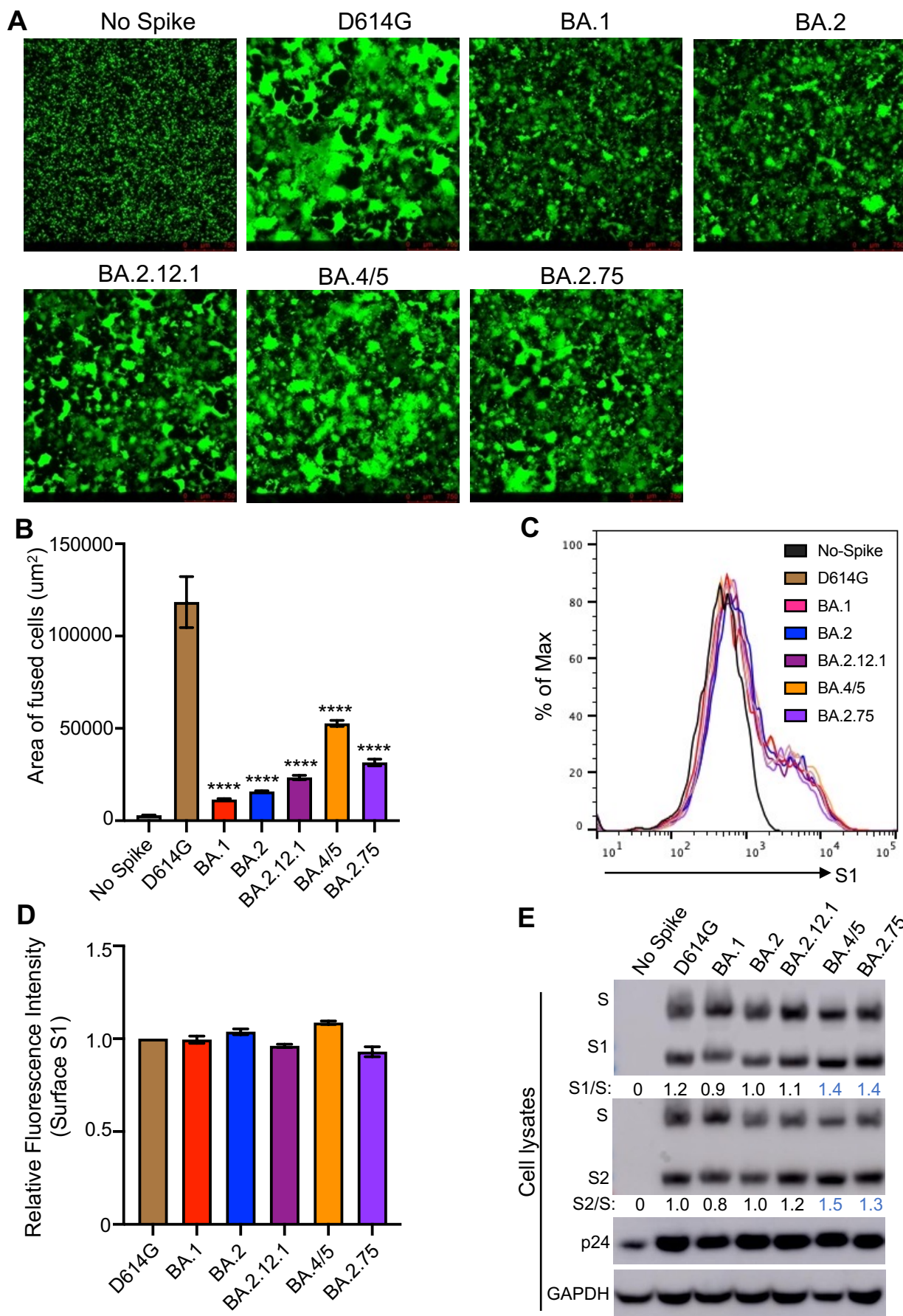


Figure 3



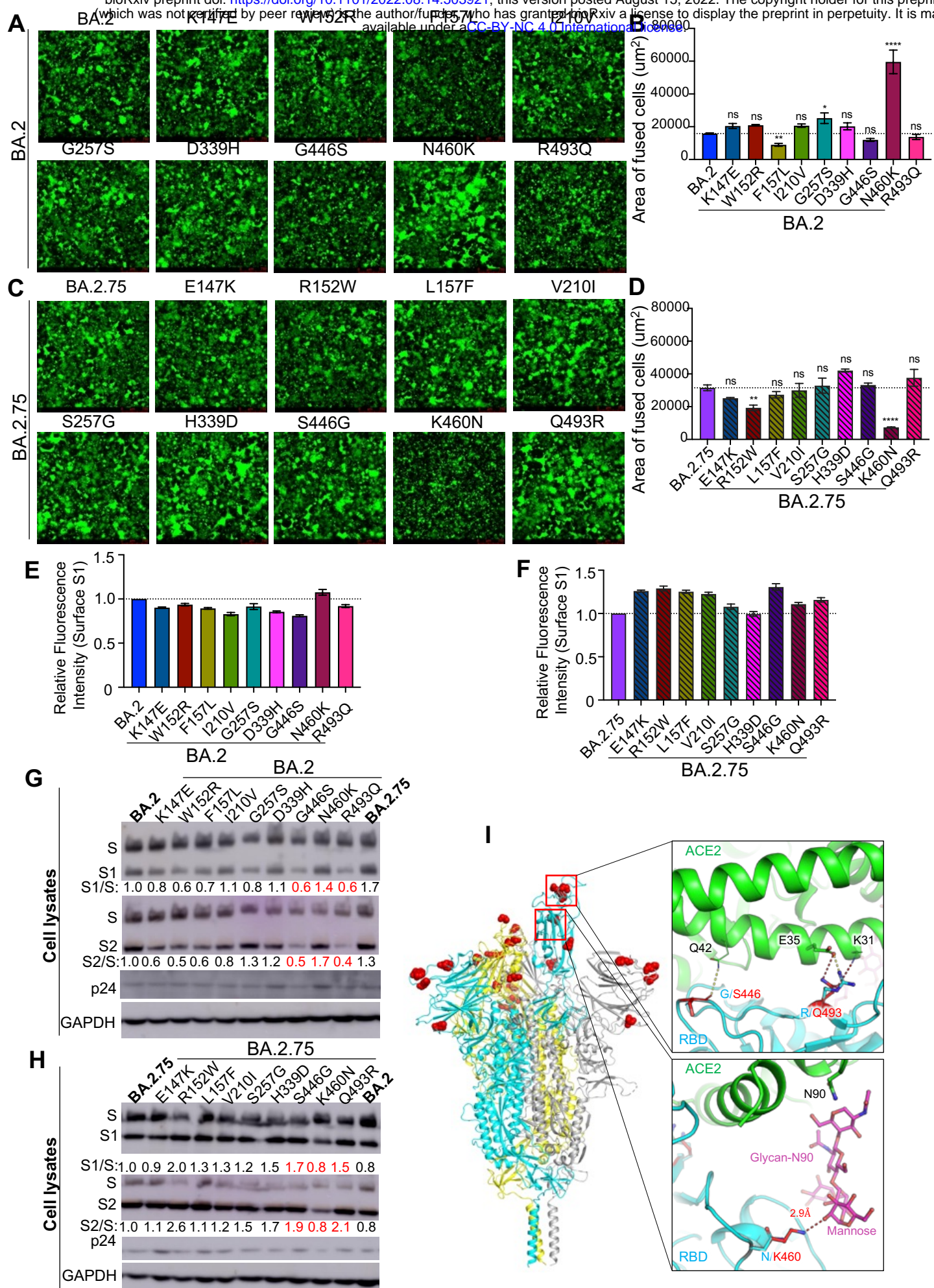


Figure 4

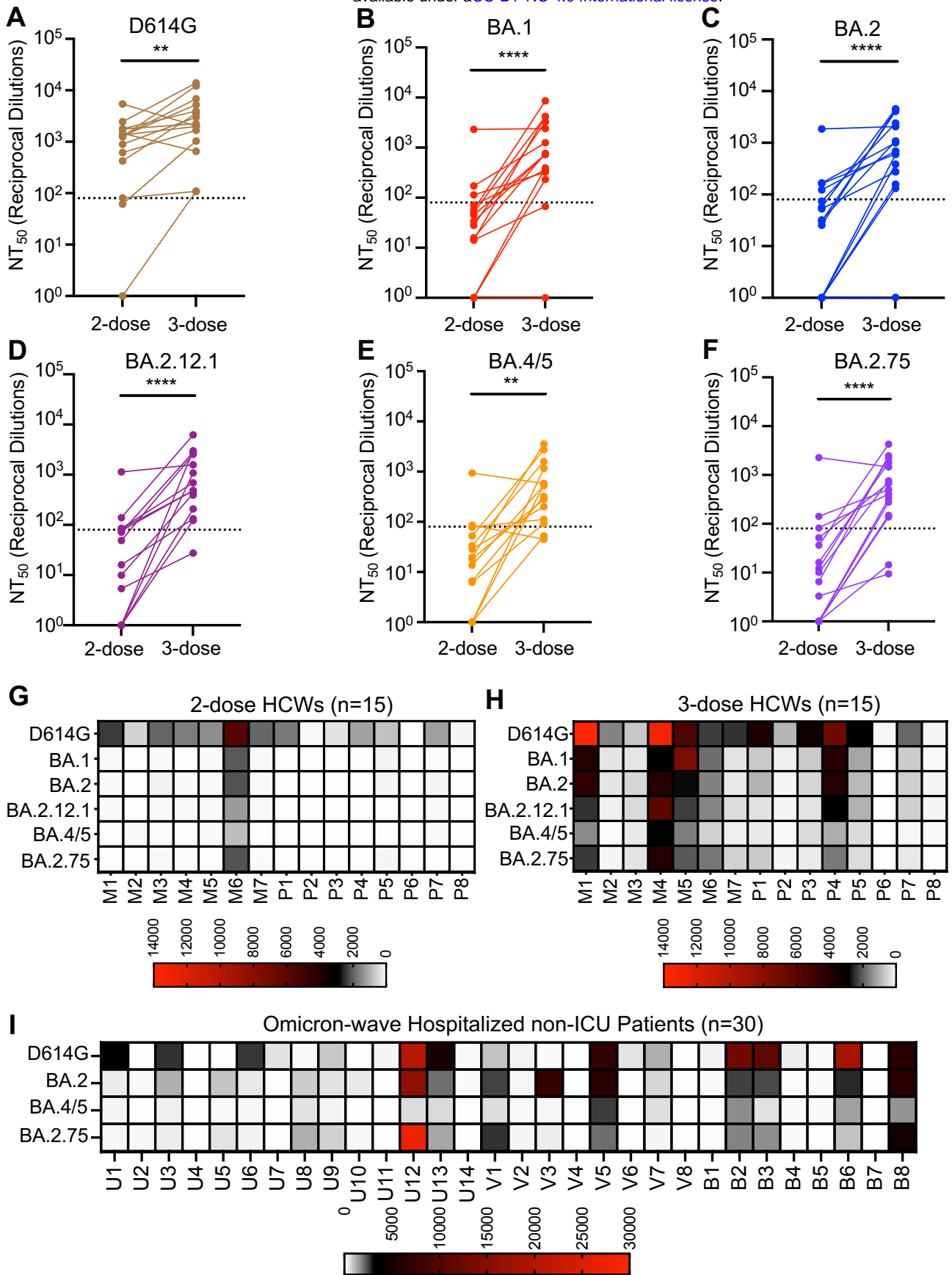


Figure S1

